Title

Automated microfluidic droplet sampling with integrated, mix-and-read immunoassays to resolve endocrine tissue secretion dynamics

Journal

Lab on a Chip, 18(19)

ISSN

1473-0197

Authors

Li, Xiangpeng
Hu, Juan
Easley, Christopher J

Publication Date

2018-09-26

DOI

10.1039/c8lc00616d

Peer reviewed

HHS Public Access

Author manuscript

Lab Chip. Author manuscript; available in PMC 2019 September 26.

Published in final edited form as:

Lab Chip. 2018 September 26; 18(19): 2926–2935. doi:10.1039/c8lc00616d.

Automated microfluidic droplet sampling with integrated, mix-and-read immunoassays to resolve endocrine tissue secretion dynamics

Xiangpeng Li[a,†], **Juan Hu**[a], and **Christopher J. Easley**[a,*]

[a]Department of Chemistry and Biochemistry, Auburn University, Auburn, AL 36849, USA.

Abstract

A fully automated droplet generation and analysis device based on pressure driven push-up valves for precise pumping of fluid and volumetric metering has been developed for high resolution hormone secretion sampling and measurement. The device consists of a 3D-printer templated reservoir for single cells or single tissue culturing, a Y-shaped channel for reagents and sample mixing, a T-junction channel for droplet formation, a reference channel to overcome drifts in fluorescence signal, and a long droplet storage channel allowing incubation for homogeneous immunoassays. The droplets were made by alternating peristaltic pumping of aqueous and oil phases. Device operation was automated, giving precise control over several droplet parameters such as size, oil spacing, and ratio of sample and reference droplets. By integrating an antibody-oligonucleotide based homogeneous immunoassay on-chip, high resolution temporal sampling into droplets was combined with separation-free quantification of insulin secretion from single islets of Langerhans using direct optical readout from the droplets. Quantitative assays of glucose-stimulated insulin secretion were demonstrated at 15-second temporal resolution while detecting as low as 10 amol per droplet, revealing fast insulin oscillations that mirror well-known intracellular calcium signals. This droplet sampling and direct optical analysis approach effectively digitizes the secretory time record from cells into droplets, and the system should be generalizable to a variety of cells and tissue types.

Introduction

Microfluidics has enabled many high-resolution temporal studies of dynamic cellular events at the single cell or single tissue level [1], which often rely on fluorescent labelling and microscopic real-time imaging [2–8]. However, the dynamics of secreted proteins—cytokines, coagulation factors, growth factors, hormones, enzymes, and other signalling molecules—that play crucial roles in many physiological and pathological processes have been significantly less studied, largely due to the deficits in accessible analytical techniques. For

*Corresponding chris.easley@auburn.edu Phone: +1-334-844-6967.

†Current address: Department of Bioengineering and Therapeutic Sciences, University of California, San Francisco, CA 94158, USA.

Electronic Supplementary Information (ESI) available: [details of any supplementary information available should be included here]. See DOI: 10.1039/x0xx00000x

Conflicts of interest

There are no conflicts to declare.

example, direct fluorescent labelling of a protein target using GFP (green fluorescent protein) fusion [9] or genetically encoded unnatural amino acid incorporation [10] requires sophisticated genetic modifications. Alternatively, the commonly used heterogeneous immunoassays for protein quantification require multiple steps of fluid handling such as washes and separations, which are not easily transferable to microfluidic devices that are well matched to study cells. Likewise, off-chip measurement of collected microfluidic samples offers accurate quantification with standard methods; however, this approach greatly sacrifices temporal resolution.

Because of its important role in the pathogenesis of type 1 and type 2 diabetes mellitus, obesity and metabolism syndrome, insulin secreted by islets of Langerhans has become one of the most studied secreted proteins on microfluidic systems [11]. Over the years, several groups developed microfluidic devices for islet secretion studies, which generally include a single- or multiple-islet trapping mechanism, a perfusion system for fresh nutrients and various treatments, and an analytical tool to monitor the hormone concentration secreted from the islets. Compared with commonly used off-chip immunoassays for insulin quantification [12–15], on-chip detection methods require less volume of sample, thus allowing higher spatial and temporal resolution and continuous monitoring. The Kennedy group introduced and developed an on-chip capillary electrophoresis immunoassay for islet secretion sampling [16–18], ultimately demonstrating monitoring of 15 islets in parallel at 10 s sampling rate [17]. However, one disadvantage of the system is the complex flow control and electrophoresis setup including external pumps, a high-voltage power supply and electrodes, and well-controlled surface chemistry for electroosmotic fluid control. Additionally, the intermittent sampling nature of those systems may cause undersampling, and the effective temporal resolution remains at the minute scale due to dispersion effects during sampling [19]. Nonetheless, both the Kennedy [16–18] and Roper[20–22] groups have proven the utility of on-chip capillary electrophoresis immunoassays for islet secretions, confirming such microfluidic systems to be uniquely qualified for temporal studies of cells. In any such continuous flow sampling method, however, the temporal resolution will be limited by longitudinal broadening that occurs as the sample flows from the cells to the on-chip assay readout point.

Droplet based microfluidics provides an appealing way to preserve the temporal chemical information by digitizing the analogue secretion signal[23, 24]. After measuring the analytes within droplets, the secretory time record can be reconstructed. Based on this concept, we were able to indirectly study insulin secretion dynamics by measuring Zn^{2+} (cosecreted with insulin) from single islets at about one-second temporal resolution[24], although the lack of automation significantly limited adjustments available to this system. Pushing such devices to their sampling limit should theoretically permit sub-second resolution, and automated operation has been shown to offer compelling analytical enhancements [25, 26].

Homogeneous immunoassays such as the molecular pincer assay[27] and related proximity assays[28–30] allow a simple mix-and-read procedure without the necessity of on-chip separation or washing, which is ideal for microfluidic secretion sampling [19], but particularly within droplets. Compared to heterogeneous assays like the capillary electrophoresis immunoassay, application of homogeneous assays within droplets would largely simplify the

microfluidic chip design. To ensure accurate measurement, the sample/probe volume ratio, and the size of each droplet must remain consistent. Peristaltic pumping with pneumatic valves dispense a predictable volume at each pumping cycle[31], thus ensuring accurate volumetric metering in a digitally controllable way. However, fluorescent based detection methods often suffer low frequency noise (1/f noise) introduced by optical system fluctuations or detector noise. Especially at low signal levels, noise is often indistinguishable from signals. Previously, our group developed a lock-in droplet detection system [32], which modulated a reference signal at the same frequency and phase as the sample by alternatively making sample and reference droplets. Highly, sensitive absorbance [32] and fluorescence [25, 26] detection were achieved with this phase-locked droplet system (μChopper), even at very short optical path lengths (tens of micrometres). Unfortunately, for homogeneous fluorescence immunoassays to be quantified with this lock-in system, a limitation of our previous design is that detection immediately followed droplet formation, which does not allow for the incubation requirement of the immunoassays.

In this work, we developed a unique microfluidic system integrating precise peristaltic pumping, a simple homogeneous immunoassay, sensitive lock-in droplet detection, and a long incubation channel for information storage. By adding the long channel for droplet storage in this new design, information on hormone secretion dynamics could be digitally saved within droplets and measured after the proper incubation time (~30 min). The device permits direct secretion sampling from single islets, mixing with assay probes, droplet formation, incubation, and detection with phase-locked referencing. While this system should be appropriate for a number of cell or tissue types, we validate the methodology with high resolution measurement of insulin secretion oscillations from pancreatic islets.

Experimental section

Microfluidic Device Fabrication with 3D-printed Templating.

Microfluidic devices were made by standard multilayer soft lithography methods[31, 33], with 3D-printed templating[14, 34–36] of the tissue culture interfaces. For detailed steps, see the supporting information (Figure S-1).

Automated Flow Control Interface.

Pneumatic valves were actuated with solenoid switches (LHDA0533115H, The Lee Co., Westbrook, CT) controlled by a multifunction data acquisition system (PCI-6259, National Instruments) and using an in-house nitrogen source adjusted to 30 psi with a pressure regulator. The 15 control channels were connected to the corresponding solenoid switches with hollow steel tubing from 22 gauge blunt syringe needles (JG22–0.5HP-90, JensenGlobal, Santa Barbara, CA) through Tygon tubing (0.02 inch ID, 0.06 inch OD, Cole-Parmer, Vernon Hills, IL). Dead-end control channels were filled with water to prevent air leakage through PDMS membranes. As a given solenoid switch was activated, nitrogen gas pressurized a lower layer control channel and closed the fluidic channel in the upper layer (push-up valves). Valve actuation timing was regulated through an in-house written LabVIEW application on a PC (for program details see Figure S-2). Peristaltic pumping occured during three-valve actuation in a 6-step pattern (101, 100, 110, 010, 011, 001), or a

5-step pattern (100, 110, 011, 001, 101), where 0 and 1 represent open and closed valves, respectively. Device operation is depicted in ESI (Video S-1).

Microfluidic Device Characterization.

The sample and probe ratio within each droplet was initially analysed by measuring the fluorescence intensity of the droplets made from fluorescein solution and buffer. The microchip with all control lines connected was taped on the microscope stage. 100 nM fluorescein in PBS buffer (pH 7.4, 0.1% BSA) was loaded into both reference and probe reservoirs, PBS buffer with 0.1% BSA was loaded into the cell culturing reservoir, perfluorocarbon oil (Novec 7500, 3M, St. Paul, MN) with 1% surfactant (Pico-Surf 1, Dolomite, Royston, UK) was loaded into the oil reservoir. Vacuum was applied at the outlet using a syringe, and valves were opened sequentially to remove air trapped in channel and to let fluids from oil, cell culturing, probe, reference, and oil to flow through the channel. The vacuum syringe was detached and the end of Tygon tubing connecting to the outlet was placed in a waste collection bottle. Droplets were then formed by running the droplet-formation mode of the LabVIEW application. Parameters for droplet formation were adjusted in the LabVIEW application front panel (for example, pumping frequency, cycles, sample/reference ratio, etc.) to acquire droplets with consistent sizes, ratio, and spacing. Fluorescence images of droplets were measured (Nikon Ti-E, inverted fluorescence microscope), and images were analysed using ImageJ and Microsoft Excel.

The peristaltic pumping-induced chaotic advection-based mixing of sample and probe solutions was studied by fluorescence imaging of fluorescein solution during mixing with buffer within the microchannel. 100 nM fluorescein in PBS buffer (pH 7.4, 0.1% BSA) and PBS buffer with 0.1% BSA were loaded into the probe reservoir and cell culturing reservoir, respectively. The LabVIEW application was set to chip characterization mode, and fluids from each individual reservoir were pumped to the droplet storage channel continuously. Fluorescent images were taken at various locations in the channel, and images were analysed using ImageJ and Microsoft Excel.

Sampling temporal resolution of the device was studied by mimicking insulin secretion. FITC-labeled insulin was pulsed into the islet culturing chamber, and the recovery of FITC-insulin into sampled droplets was measured by fluorescence imaging. 100 nM FITC-insulin in PBS buffer (pH 7.4, 0.1% BSA) and PBS buffer with 0.1% BSA were loaded into the probe reservoir and cell culturing reservoir, respectively. The LabVIEW application was set to islet mimicking mode, and the FITC-insulin solution was pumped 20 cycles to prime the tissue culture side (right) of the Y-channel. Extra FITC-insulin in the islet chamber was washed with PBS buffer 3 times by pipetting. After pumping the FITC-insulin solution into the islet chamber for one additional pump cycle, then waiting for varying times from 1 to 20 s, the solution was pumped from the islet reservoir to the incubation channel while the fluorescence imaging was taken. Images were analysed using ImageJ and Microsoft Excel.

Extraction of Primary Islets.

All experiments involving animals (mice, C57BL/6J) were performed in compliance with relevant laws and institutional guidelines and were approved under protocol numbers 2014–

2096 or 2017–3101 by the institutional animal care and use committee (IACUC) of Auburn University. Pancreatic islets were extracted as described previously[37, 38] from 18–20 week old male C57BL/6J mice (Jackson Laboratories). Following isolation, islets were placed in RPMI media (10% FBS, 11 mM glucose) at 37 °C and 5% CO_2 to incubate overnight.

Islet Secretion and Insulin Quantification.

Insulin was quantified using a homogeneous fluorescence assay (Human Insulin FRET-PINCER Assay Kit; Mediomics, St. Louis, MO) within droplets. The microchip was mounted within a microscope stagetop incubator (Tokai Hit, Japan) held at 37 °*C*. 50 μL of pincer assay probe mixture (Antibody A and B, 16-fold concentration of the kit suggested level) was loaded in the probe reservoir, and 50 μL of probe mixture (8-fold concentration of the kit suggested level) was loaded into the reference reservoir to serve as the reference. 10 μL of mineral oil was added on top of both probe and reference reservoirs to prevent evaporation during the prolonged experiment at 37 °*C*.

BMHH buffer (3.5 mM glucose, 0.1% BSA) was added into the islet reservoir. After air removal and channel priming with oil, a single islet (pre-starved for 30 min in BMHH buffer with 3.5 mM glucose and 0.1% BSA) was carefully loaded into the islet chamber at the bottom of the reservoir using a 2 μL pipette guided with the microscope. Next, sample droplets and reference droplets were alternatively formed with the droplet formation mode of the LabVIEW application. After 15 min, the buffer was quickly changed to a high glucose buffer (19.5 mM glucose in BMHH with 0.1% BSA) by gentle pipetting to avoid disturbing the trapped islet. After another 20 min, the buffer was changed back to 3.5 mM glucose to treat the islet for another 10 min. Droplets were continuously formed as the buffer was changed. Once the glucose stimulation was completed, the incubator was switched off to cool the system back to room temperature, and specially sequenced droplets were generated (for example 1 reference after 3 sample droplets) to serve as an addressing code for time stamping in subsequent analysis. The islets were removed, and various concentrations of insulin (0, 32, 64, 128, 256, 512, 902.5 ng/mL) were loaded to generate a standard curve. Droplets were generated for 10 min at each concentration before changing to next level of insulin. As the droplets formed, fluorescence imaging was performed (Nikon Ti-E, 40X objective lens through FITC filter cube) at the imaging region, where all droplets passed through sequentially.

For additional islet analyses, the stagetop incubator was turned to 37 °*C*, the temperature was equilibrated, and the above procedures were repeated. One calibration curve was made after each islet sampling experiment, and each islet was sampled and analysed with a new device. For all experiments, sample droplets and reference droplets were intentionally controlled to be different sizes for easy identification during analysis. Images were analysed with ImageJ and Microsoft Excel for insulin quantification.

Results and Discussion

Microfluidic Device Design

As shown in Figure 1 and Figure S-3, the microfluidic device consisted of several components: (1) Y-shaped channel for reagent and sample mixing; (2) T-junction channel for droplet formation; (3) reference channel for reference droplet generation used for phase-locked detection; (4) long incubation channel for droplet storage and imaging; (5) 3D-templated reservoir for tissue culturing; and (6) pneumatic control channels for fully automated chip operation (Figure S-3).

One key feature of the device is that all fluid is moved through channels by three-valve peristaltic pumps[31]. In each pumping cycle, the net volume dispensed downstream can be closely estimated by the volume occupied by the center valve membrane upon closing, thus the sample volume could be accurately controlled by pumping a specified number of cycles. For the oil and reference pumps, the fluidic channels above the center valves were widened (Figure S-3A) to allow more rapid pumping during these steps of the workflow. To further optimize the peristaltic pump flow rates, we tested two different pumping patterns: a 5-step pattern (100, 110, 011, 001, 101) and a 6-step pattern (101, 100, 110, 010, 011, 001), where 0 and 1 represent open and closed valves, respectively. Since both pumping patterns were found to dispense equal volumes in each cycle, the 5-step pattern was used in all experiments because it required less time per cycle, thereby increasing the effective flow rate. Compared to more passively controlled or off-chip driven microfluidic systems—using syringe pumps, electroosmosis, pressure, or vacuum that all rely on laminar flow to control the ratio of mixed components—these peristaltic pumps have been validated for highly precise and automated control[26, 31, 39] over the volume metered per pump cycle (Figure S-3). The valves also did not suffer from low frequency fluctuations in metering, and the pulsed flow nature of pumping facilitated mixing of the two components from both side of the Y-channel through chaotic advection. As shown in Figure 2C, the fluorescent solution from the left side of the Y channel and buffer from the right side were well mixed when they reached the downstream T-junction channel. The zig-zag channel[23] at the beginning of incubation channel also ensured mixing after droplets were formed, without compromising temporal resolution.

The long droplet incubation channel was templated with SU-8 photoresist (shown in orange in Figure 1) instead of AZ photoresist for the following three reasons. First, unlike the rounded AZ patterned channel, the squared channel provided improved, more predictable fluorescence imaging quality. Second, the two-step patterning allowed different depths for the droplet formation channel and droplet storage channel. Thus, deeper channels could hold more droplets and allow more information buffering. Third, the squared profile (Figure S-4) helped maintain spacing between droplets to ease data analysis and prevent unwanted merging. It is noteworthy that this deeper incubation channel was not made deep enough to cause any droplet reordering, thus the temporal sequence of droplets was retained in our system (see Figures S-6 and S-7).

To successfully generate droplets, the continuous phase (oil in our case) must effectively wet the channel surface. As a hydrophobic material, PDMS is ideal for water-in-oil droplet

generation. Plasma oxidization treatment for bonding the PDMS to glass slides produced transient hydrophilic surfaces, but the surface slowly recovered to be hydrophobic because of the migration of the uncured monomers[40]. Thermal aging facilitated this process while also curing most remaining monomers to prevent leaching into cell culturing buffer. An earlier design iteration (Figure S-5) included a shorter connection between the Y-channel and T-junction and no gating valves. Attracted by the wettability of PDMS surface and partially due to the pulsing nature of pumped flow, the oil adhered to the channel surface and slowly migrated into the Y-channel. Consequently, unwanted smaller droplets formed. To avoid this, the Y-channel was moved further away (15 mm) from the T-junction, and gating valves were added (Figures S-4 and S-5).

Automated droplet formation.

The custom LabVIEW application was programmed to alternatively pump aqueous and oil fluids to generate droplets (see Figure S-2), allowing control over several droplet parameters. The droplets' size was changeable by pumping aqueous phase for more or less cycles, the spacing in between droplets was controlled by varying the pump cycles of the oil phase, and the sample and reference droplet ratio as well as the droplet generation frequency were also controllable by the pumping codes (Figure S-6). These features were analogous to those reported by Zeng et al. using normally closed valves in PDMS/glass devices [39]. Since droplet formation was digitally controlled, and the droplets were sequentially sent into the storage channel, the incubation times of each droplet were individually addressable. Ideally, as droplets passed through the detection region, all the components inside each droplet had reacted for the same time period. Due to the smaller oil fluidic resistance, the space in between droplets was observed to decrease as the droplets advanced downstream, particularly if the droplets were small. This issue was partially solved by using SU-8 patterned, rectangular channels. Another solution was alternatively making large and small droplets, which paired up during flow downstream (Figure S-7) and allowed easier data analysis. Finally, it should be noted that during long term experiments, it was important to regularly empty the outlet reservoir to avoid build-up of hydraulic pressure differentials that affected device performance.

It is worth mentioning that the droplet formation mechanism was different from T-junction, co-flow, flow-focusing, step emulsification, or other reported mechanisms[41] . As the oil wet the hydrophobic PDMS surface, a small amount of oil was confined in between the membranes above the sample and reference gate valves. After pumping aqueous solution, the gate valve closed and created a new oil-water interface formation. Compared with the passive T-junction droplet formation mechanism, which can suffer from droplet size variations caused by pressure and flow rate differences, the valve segmentation-based droplet formation method used herein has been proven by our group and others[26, 31, 39] to provide accurate and precise volumetric control of droplets.

Mixing Ratio Consistency.

Consistent sample and probe mixing ratio within each droplet is crucial for droplet immunoassay accuracy. The mixing ratio was measured by fluorescence imaging of sample droplets made from fluorescein solution mixed with buffer and reference droplets made with

undiluted fluorescein solution. As shown in Figure 2A-B, after characterizing 33 droplets of each type, the fluorescent intensity of mixed sample droplets was 48.05 ± 0.22% of the reference droplets, which indicated the mixing ratio was 1 : 1.08. This mixing ratio was nearly 1 : 1 as designed, and the mixing precision was high at <0.5% relative standard deviation. The peristaltic pumping also introduced chaotic advection, which helped mixing of reagents from the two sides of the Y-channel. As shown in Figure 2C, the two reagents were well mixed as they reached the T-junction channel. This accelerated mixing allowed consistent immunoassay performance within droplets.

Islet Trapping Region.

The islet must be confined within a microfluidic channel or chamber that brings nutrients to and hormone from the tissue, or the hormones will diffuse into the bulk solution, and temporal dynamic information will be lost. Previously, we used a deep microchannel for islet trapping[12], which was interfaced with the solution reservoir via a 1.5 mm hole. Here, by simply making the interfacing hole with a 500 μm punch, a vertical microfluidic channel for islet trapping was created and interfaced with the wide area (300 μm diameter) of the fluidic channel to prevent islet loss downstream (see Figure S-8). A typical islet chamber was 500 μm in diameter and 500 μm in depth, and the total volume was about 100 nL. As solution in the reservoir was changed by pipette, the solution within the islet chamber was completely switched to the stimulant solution within 2–3 min (refer to Figure 4C), although sampling shows that the islets begin experiencing a stimulant gradient within seconds, as we have previously shown [12]. The islets were not disturbed when the solution was gently removed and added.

Temporal Resolution Assessment by Mimicking Insulin Secretion.

Since the device operated by alternatively pumping aqueous solution and oil, the insulin secreted by an islet in the culture chamber was sampled into the droplets only when sample pumping was active. During the rest of the droplet formation cycle, the secreted insulin was freely diffusing into the islet trapping region and perhaps into the bulk reservoir, which would degrade the temporal resolution of cell sampling. It was therefore deemed important to carefully evaluate the device's temporal resolution. Fortunately, the on-chip valves enabled a unique experiment to be devised for this purpose. We chose to reprogram the device operation—for characterization only—to dispense short pulses of dye-labeled insulin into the islet trapping region, wait for varying time periods, then sample from this chamber. As detailed below, this experiment enabled an accurate assessment of the device's operating temporal resolution while also predicting its resolution limits.

To evaluate the temporal resolution of our system, the diffusion and sampling of insulin was tested with the custom islet mimicking mode of the LabVIEW application (Figure 3A-B, details of workflow are in Figure S-2). FITC-insulin was pumped into the islet trapping region, left to diffuse for varying times (1 to 30 s), then sampled into the channel. Assuming the islet is a sphere with 150 μm diameter (a normal islet size is in between 100–200 μm[12]), the volume of an islet is ~1.7 nL. To pump a similar ~1.8 nL as a short burst into the culture chamber, our device required 5 pump cycles (dispensing volume of each cycle = 0.365 nL, Figure S-3B). During the varying incubation times that followed, the fluorescence intensity

decreased at the expected exponential decay with 10.5 s half-life (upper bound of curves in Figure 3C). Upon subsequent sampling out of the chamber using peristaltic pumping, the fluorescence intensity decreased at a faster rate (exponential decay with 1.4 s half-life). The time for sampling half of the FITC-insulin into the sampling channel was plotted as t_{FWHM} (blue curve) in Figure 3D. Notably, this time (t_{FWHM}) represented the time separation needed to distinguish two equivalent insulin pulses secreted by an islet in the trapping region. The varied incubation time ($t_{incubation}$) in this experiment served to mimic the waiting time needed to form oil and reference droplets, and this was plotted in Figure 3D as well (gray curve). The best temporal resolution for each tested condition (t_{maxRes}; orange curve) was therefore equal to the sum: $t_{maxRes} = t_{incubation} + t_{FWHM}$.

These data have important implications. First, with longer incubation times, the contribution of free diffusion (t_{FWHM}) to the ultimate temporal resolution (t_{maxRes}) was minimized (inset right). In our current system, the temporal resolution was determined to be 15 seconds, and this value was mainly defined by the time needed for making droplets (dispensing oil and aqueous phases for sample and reference droplets). Secondly, the data suggest a means for improving the resolution in future devices. If we optimize the device to more rapidly pump oil and reference droplets (thereby reducing $t_{incubation}$ in Figure 3D), this device could feasibly approach a resolution limit of merely 2 seconds (lowest orange point in inset left plot, Figure 3D).

Insulin Quantification within Droplets.

Previously, we reported an automated microfluidic sample chopper (μChopper) which was successfully used for insulin quantification within droplets by using a fluorescence quenching based homogeneous immunoassay[25]. This μChopper was not able to mix the sample and immunoassay probes, nor accomplish on-chip incubation. Thus, all the samples were premixed and incubated before loading onto the μChopper. However, an important feature of the μChopper is the ability discriminate very small differences in optical signals (fluorescence[25, 26], absorbance[32]) even with high background or at very low concentrations due the drift correction and $1/f$ noise reduction. This concept was used herein and was very important for enabling insulin secretion quantification from single islets.

Our device allowed automated, continuous droplet formation with islet sampling and assay probes at a consistent ratio (see Video S-1 in ESI). The droplets formed were also able to be stored within the incubation channel to meet the assay reaction time requirements (~30 min in this case) for signal accumulation. Firstly, the assay performance was tested by manually changing the insulin solution (0, 32, 64, 128, 256, 512, and then back to 0 nM) within the reservoir, where diluted assay probe was used as the constant reference. As shown in Figure 4, the fluorescence intensity of sample droplets decreased as the insulin concentration increased (blue data), while that of reference droplets (orange data) held within a narrow range, albeit with some drift. This fluorescence quenching effect was proportional to insulin concentration (Figure 4B-D), and signal drifts were effectively corrected by our lock-in analysis method [25, 26, 32]. The limit of detection (LOD) was calculated to be 30 ng/mL (or 5 nM), and the mass LOD was 10^{-17} mol (10 amol) with each pair of droplets. Upon solution changing, the fluorescence ratio between sample and reference quickly equilibrated within

2–3 min (Figure 4C), as discussed above. Note that this 2–3 min exchange time represented the stimulant exchange time in the bulk reservoir, not the temporal sampling resolution into droplets (15 seconds). The stepwise data analysis procedure is shown in Figure S-9.

Single Islet Insulin Secretion Dynamics.

In pancreatic islets, insulin secretion is synchronized with the elevation of cytosolic Ca^{2+} levels throughout the electrically coupled cell clusters at high glucose levels. During the glucose-induced insulin secretion process, the uptake of glucose into β-cells through glucose transporter GLUT2 increases the production of ATP via the glycolytic pathway and tricarboxylic acid (TCA) cycle. The increased ATP/ADP ratio closes the ATP-sensitive K^+ channels, and the decreased K^+ permeability leads to membrane depolarization. Consequently, the voltage-dependent Ca^{2+} channel opens, Ca^{2+} influx occurs, and the increased Ca^{2+} concentration triggers the exocytosis machinery of insulin granules. It is known that insulin secretion is a pulsatile phenomenon with three types of oscillations: regular and slow (frequency of ~ 0.2 min^{-1}), regular and rapid (frequency of 2–3 min^{-1}), or mixed, in which rapid oscillations are superimposed on slow ones[42].

The slow oscillations of insulin secretion were observed by several others using direct insulin immunoassays on microfluidic devices[16]. However, fast oscillations of insulin were only directly observed by proinsulin genetic GFP and mCherry fusions and total internal reflection fluorescence microscopy[43]. Other observations of the rapid oscillation rely on indirect measurement, such as fluorescence Ca^{2+} imaging [42–45], electrophysiology analysis of membrane potential using patch clamp[46], or Zn^{2+} quantification [24] (ions co-released at 2:6 ratio with insulin).

To test if our device was capable of observing the rapid oscillation of insulin secretion, single islets' dynamic insulin secretions were measured during treatment with approximate square waveforms of physiologically relevant levels of glucose. Single islets were loaded into the trapping chamber (Figure S-10), and droplets containing both the secretome and assay probes were continuously made at ~ 0.1 Hz and allowed to incubate for downstream analysis. By constantly referencing to the droplets precisely made with diluted assay probe (μChopper concept), the insulin secretions were precisely quantified after assay incubation and storage in the long channel. The homogeneous immunoassay we used is based on a pair of oligonucleotide-conjugated antibodies targeting insulin, where the proximity effect brought together a fluorophore/quencher pair [25, 27, 47]. Consequently, the base pairing of complimentary probes was tuned for room temperature performance. Since islets required culture at 37 °C, we measured droplets' fluorescence intensities after equilibrating the device to room temperature. The long droplet storage channel could hold >2000 droplets (> 2 h information storage), thus we were able to finish a standard curve and single islet secretion dynamics studies in each run. In the future, the assay optimal temperature can also be tuned to 37 °C by optimizing the hybridization energies [30], which should allow longer-term monitoring.

In the tissue-sampling experiments, glucose-induced insulin secretion from single islets was observed to generally follow the input glucose waveforms, as expected. Additionally, as shown in Figure 5, the islets exposed to low level glucose (3.5 mM) exhibited insulin

secretion oscillations with periods of 20–30 s at low magnitude (0.7, 0.3, and 0.35 pg/islet/min for Figure 5 A, B, and C, respectively). Upon high glucose treatment (19.5 mM), the oscillation magnitude increased to more than double compared to that with low glucose treatment, and the oscillations with longer periods (~1 to 3 min) became dominant. In fact, the histograms in Figure 5 (right) show that our unique micro-analytical system revealed a significant count of sub-minute (~20–60 s) oscillations or bursts of insulin from all tested islets. The periods of these fast oscillations matched very well with the known calcium oscillations within islets[24, 42], providing direct hormone sampling evidence of the coupling between cellular Ca^{2+} levels and insulin exocytosis.

Thus, our novel microanalytical system enabled clear observation of the mixed oscillation type in single C57BL/6J murine islets, where fast insulin oscillations were superimposed on slow ones[42]. Interestingly, the average insulin secretion rates, ranging from near zero to just above 1 pg $islet^{-1}$ min^{-1}, were somewhat lower than previous reports using islets from this mouse strain[12, 34]. While the reasoning for this difference is not yet clear, the ability of the device to capture expected glucose-stimulated secretion was encouraging. It was even possible to quantitatively analyse individual bursts of secreted insulin, as shown in the zoomed inset of a 5-minute data segment in Figure 5B. In this example, just after glucose was increased, two well-resolved bursts of insulin were trapped into 12 droplets, and our analysis revealed the release of 2.10 pg (361 amol) and 1.25 pg (215 amol) of insulin in the two sequential bursts, respectively. These results confirmed our device to be uniquely suited for automated, high temporal resolution studies on hormone secretion dynamics.

Conclusions

A microfluidic droplet generator using on-chip peristaltic pumping for accurate fluid metering was developed and proven feasible for analysing high temporal resolution insulin secretion dynamics from single islets. Because the sampling method and immunoassay are generalizable, these results suggest the device should be translatable to study secretion dynamics of other proteins (e.g. cytokines, coagulation factors, hormones, enzymes, growth factors, etc.) or to sample from other tissues or cell types. The device could also be integrated with other microfluidic modules, like controllable perfusion systems for tissue and cell culturing [14, 48–53] for automated stimulation. With the addition of more probe input channels and integration of fluorescence- or absorbance-based coupled enzyme assays, it should also be possible to monitor secretion of small molecules in the future. Our device can be considered as a fluidic analogue-to-digital converter that digitizes the secretory time record from cells into droplets.

Compared with other microfluidic droplet generators that allow kHz droplet formation frequencies[41], our device only forms droplet at a frequency up to ~1 Hz due to the slow pneumatic valve actuation and relatively small dispensing volume per pumping cycle. To improve the sampling rate without sacrificing the sensitivity, sophisticated droplet manipulation technologies, such as droplet merging[54] or pico-injection[55], could be integrated into our device for introducing reagents into sample droplets. This would also help multistep immunoassays or enzyme-based assays to be transferred into the microfluidic droplet system in a more controllable manner. A microfluidic first-in-first-out droplet shift

register[56] could also be useful to synchronize the detection of droplets, which would allow in line data collection within the software and largely simplify the data analysis.

Supplementary Material

Refer to Web version on PubMed Central for supplementary material.

Acknowledgements

Support for the work was provided by the National Institutes of Health (R01 DK093810) and the Department of Chemistry and Biochemistry at Auburn University.

Notes and references

1. Duncombe TA, Tentori AM and Herr AE, Nature reviews. Molecular cell biology, 2015, 16, 554–567. [PubMed: 26296163]
2. Kellogg RA, Tian C, Lipniacki T, Quake SR and Tay S, eLife, 2015, 4, e08931. [PubMed: 26488364]
3. Jovic A, Wade SM, Neubig RR, Linderman JJ and Takayama S, Integrative biology : quantitative biosciences from nano to macro, 2013, 5, 932–939. [PubMed: 23732791]
4. McClean MN, Hersen P and Ramanathan S, Cell cycle (Georgetown, Tex.), 2009, 8, 373–376.
5. Gubelmann C, Waszak SM, Isakova A, Holcombe W, Hens K, Iagovitina A, Feuz JD, Raghav SK, Simicevic J and Deplancke B, Molecular systems biology, 2013, 9, 682. [PubMed: 23917988]
6. Geertz M, Shore D and Maerkl SJ, Proceedings of the National Academy of Sciences of the United States of America, 2012, 109, 16540–16545. [PubMed: 23012409]
7. Chiang YY and West J, Lab on a chip, 2013, 13, 1031–1034. [PubMed: 23385220]
8. Tay S, Hughey JJ, Lee TK, Lipniacki T, Quake SR and Covert MW, Nature, 2010, 466, 267–271. [PubMed: 20581820]
9. Tsien RY, Annual review of biochemistry, 1998, 67, 509–544.
10. Liu W, Brock A, Chen S, Chen S and Schultz PG, Nature methods, 2007, 4, 239–244. [PubMed: 17322890]
11. Schrell AM, Mukhitov N, Yi L, Wang X and Roper MG, Annual review of analytical chemistry (Palo Alto, Calif.), 2016, 9, 249–269.
12. Godwin LA, Pilkerton ME, Deal KS, Wanders D, Judd RL and Easley CJ, Analytical chemistry, 2011, 83, 7166–7172. [PubMed: 21806019]
13. Lee D, Wang Y, Mendoza-Elias JE, Adewola AF, Harvat TA, Kinzer K, Gutierrez D, Qi M, Eddington DT and Oberholzer J, Biomedical microdevices, 2012, 14, 7–16. [PubMed: 21850483]
14. Li X, Brooks JC, Hu J, Ford KI and Easley CJ, Lab on a chip, 2017, 17, 341–349. [PubMed: 27990542]
15. Lo JF, Wang Y, Blake A, Yu G, Harvat TA, Jeon H, Oberholzer J and Eddington DT, Analytical chemistry, 2012, 84, 1987–1993. [PubMed: 22296179]
16. Dishinger JF, Reid KR and Kennedy RT, Analytical chemistry, 2009, 81, 3119–3127. [PubMed: 19364142]
17. Nunemaker CS, Dishinger JF, Dula SB, Wu R, Merrins MJ, Reid KR, Sherman A, Kennedy RT and Satin LS, PloS one, 2009, 4, e8428. [PubMed: 20037650]
18. Roper MG, Shackman JG, Dahlgren GM and Kennedy RT, Analytical chemistry, 2003, 75, 4711–4717. [PubMed: 14674445]
19. Schrell AM, Mukhitov N, Yi L, Adablah JE, Menezes J and Roper MG, Anal. Methods, 2017, 9, 38–45. [PubMed: 28458724]
20. Lomasney AR, Yi L and Roper MG, Analytical chemistry, 2013, 85, 7919–7925. [PubMed: 23848226]

21. Mukhitov N, Yi L, Schrell AM and Roper MG, Journal of chromatography. A, 2014, 1367, 154–160. [PubMed: 25263064]
22. Yi L, Wang X, Dhumpa R, Schrell AM, Mukhitov N and Roper MG, Lab on a chip, 2015, 15, 823–832. [PubMed: 25474044]
23. Song H and Ismagilov RF, Journal of the American Chemical Society, 2003, 125, 14613–14619. [PubMed: 14624612]
24. Easley CJ, Benninger RK, Shaver JH, Steven Head W and Piston DW, Lab on a chip, 2009, 9, 1119–1127. [PubMed: 19350094]
25. Negou JT, Avila LA, Li X, Hagos TM and Easley CJ, Analytical chemistry, 2017, 89, 6153–6159. [PubMed: 28467848]
26. Negou JT, Hu J, Li X and Easley CJ, Anal Methods, 2018, DOI: DOI: 10.1039/C8AY00947C.
27. Heyduk E, Dummit B, Chang YH and Heyduk T, Analytical chemistry, 2008, 80, 5152–5159. [PubMed: 18491925]
28. Hu J and Easley CJ, Analytical chemistry, 2017, 89, 8517–8523. [PubMed: 28696682]
29. Hu J, Kim J and Easley CJ, Anal Methods, 2015, 7, 7358–7362. [PubMed: 26366207]
30. Kim J, Hu J, Bezerra AB, Holtan MD, Brooks JC and Easley CJ, Analytical chemistry, 2015, 87, 9576–9579. [PubMed: 26372070]
31. Unger MA, Chou HP, Thorsen T, Scherer A and Quake SR, Science (New York, N.Y.), 2000, 288, 113–116.
32. Deal KS and Easley CJ, Analytical chemistry, 2012, 84, 1510–1516. [PubMed: 22191400]
33. Thorsen T, Maerkl SJ and Quake SR, Science (New York, N.Y.), 2002, 298, 580–584.
34. Brooks JC, Ford KI, Holder DH, Holtan MD and Easley CJ, The Analyst, 2016, 141, 5714–5721. [PubMed: 27486597]
35. Brooks JC, Judd RL and Easley CJ, Methods in molecular biology (Clifton, N.J.), 2017, 1566, 185–201.
36. Godwin LA, Brooks JC, Hoepfner LD, Wanders D, Judd RL and Easley CJ, The Analyst, 2015, 140, 1019–1025. [PubMed: 25423362]
37. Karl RC, Scharp DW, Ballinger WF and Lacy PE, Gut, 1977, 18, 1062–1072. [PubMed: 414967]
38. Stefan Y, Meda P, Neufeld M and Orci L, The Journal of clinical investigation, 1987, 80, 175–183. [PubMed: 3110211]
39. Zeng Y, Shin M and Wang T, Lab on a chip, 2013, 13, 267–273. [PubMed: 23160148]
40. Vickers JA, Caulum MM and Henry CS, Analytical chemistry, 2006, 78, 7446–7452. [PubMed: 17073411]
41. Zhu P and Wang L, Lab on a chip, 2016, 17, 34–75. [PubMed: 27841886]
42. Gilon P, Ravier MA, Jonas JC and Henquin JC, Diabetes, 2002, 51 Suppl 1, S144–151. [PubMed: 11815474]
43. Schifferer M, Yushchenko DA, Stein F, Bolbat A and Schultz C, Cell chemical biology, 2017, 24, 525–531.e524. [PubMed: 28366620]
44. Cane MC, Parrington J, Rorsman P, Galione A and Rutter GA, Cell calcium, 2016, 59, 32–40. [PubMed: 26769314]
45. Lee B, Song T, Lee K, Kim J, Han S, Berggren PO, Ryu SH and Jo J, PloS one, 2017, 12, e0172901. [PubMed: 28235104]
46. Glynn E, Thompson B, Vadrevu S, Lu S, Kennedy RT, Ha J, Sherman A and Satin LS, Endocrinology, 2016, 157, 611–623. [PubMed: 26697721]
47. Kim J, Hu J, Sollie RS and Easley CJ, Analytical chemistry, 2010, 82, 6976–6982. [PubMed: 20704387]
48. Blagovic K, Kim LY and Voldman J, PloS one, 2011, 6, e22892. [PubMed: 21829665]
49. Castiello FR, Heileman K and Tabrizian M, Lab on a chip, 2016, 16, 409–431. [PubMed: 26732665]
50. Jimenez-Valdes RJ, Rodriguez-Moncayo R, Cedillo-Alcantar DF and Garcia-Cordero JL, Analytical chemistry, 2017, 89, 5210–5220. [PubMed: 28406613]
51. Kim L, Toh YC, Voldman J and Yu H, Lab on a chip, 2007, 7, 681–694. [PubMed: 17538709]

52. Mirzaei M, Pla-Roca M, Safavieh R, Nazarova E, Safavieh M, Li H, Vogel J and Juncker D, Lab on a chip, 2010, 10, 2449–2457. [PubMed: 20714499]
53. Zhang X and Roper MG, Analytical chemistry, 2009, 81, 1162–1168. [PubMed: 19178342]
54. Mazutis L, Baret JC, Treacy P, Skhiri Y, Araghi AF, Ryckelynck M, Taly V and Griffiths AD, Lab on a chip, 2009, 9, 2902–2908. [PubMed: 19789742]
55. Abate AR, Hung T, Mary P, Agresti JJ and Weitz DA, Proceedings of the National Academy of Sciences of the United States of America, 2010, 107, 19163–19166. [PubMed: 20962271]
56. Zagnoni M and Cooper JM, Lab on a chip, 2010, 10, 3069–3073. [PubMed: 20856984]

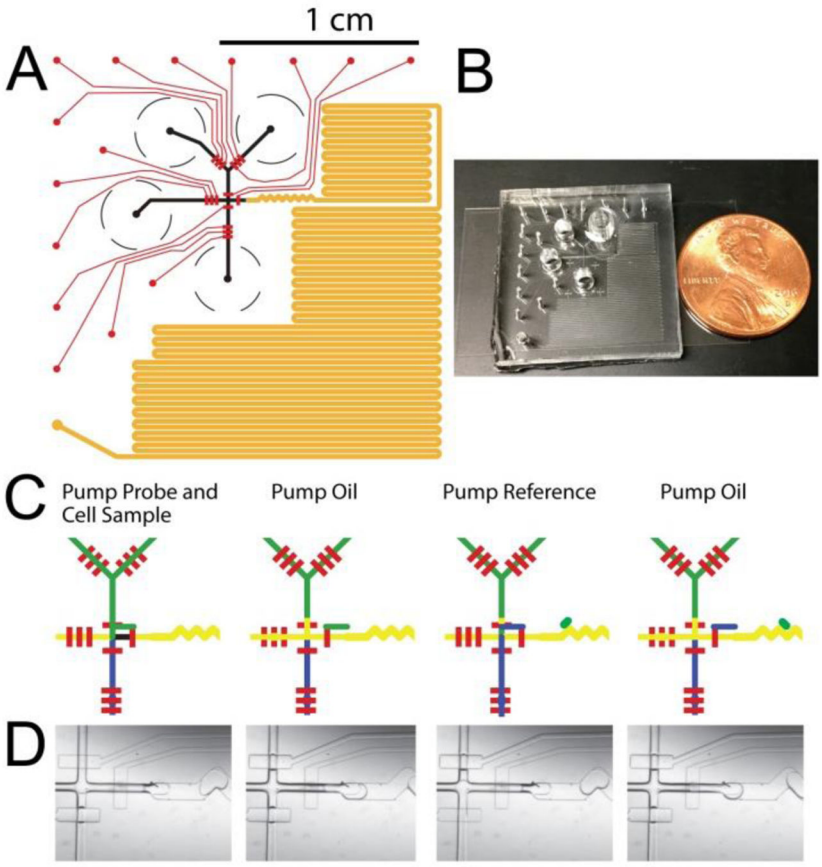

Figure 1.

(A) Schematic of microfluidic channel layouts, with rounded fluidic channels shown in black, squared fluidic channels in orange, and pneumatic control channels in red. **(B)** Photo of assembled device. **(C)** Workflow of automated droplet formation and **(D)** corresponding images of the device in each step.

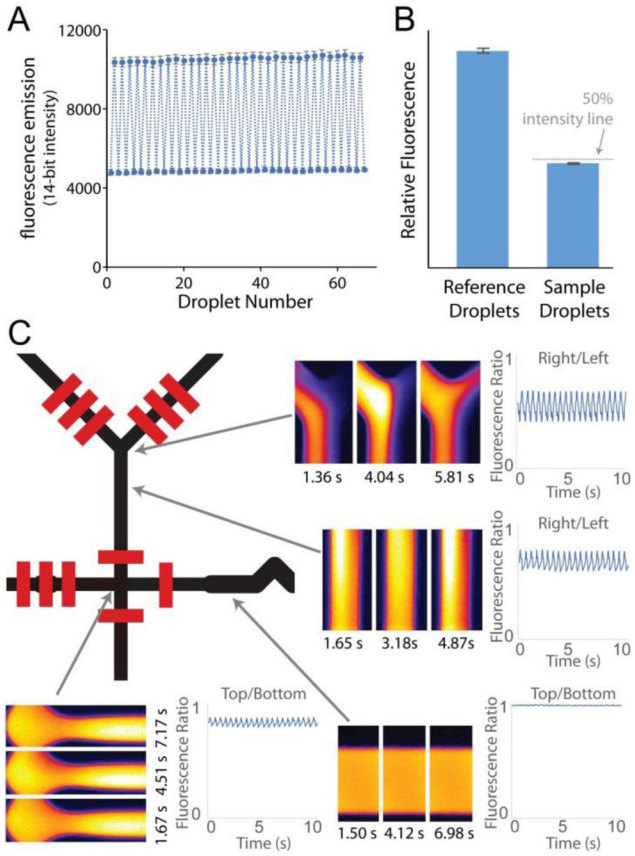

Figure 2.

Sample/probe mixing characterization. **(A)** Sample droplets made by mixing fluorescein and buffer were compared to reference droplets of fluorescein standard over time. **(B)** Averaged fluorescent intensities from reference and sample droplets showed a mixing ratio of 1 : 1.08, with precision at < 0.5%. For comparison, the position of the gray dotted line represents 50% of the reference droplet intensity. **(C)** Peristaltic pumping induced mixing via chaotic advection. Fluorescent imaging of fluorescein solution (left) mixed with buffer (right side) indicated the relative concentrations of fluorescein at various locations and times. Plots show the ratios of fluorescent intensities from right and left sides (or top and bottom sides) of the channel at corresponding locations.

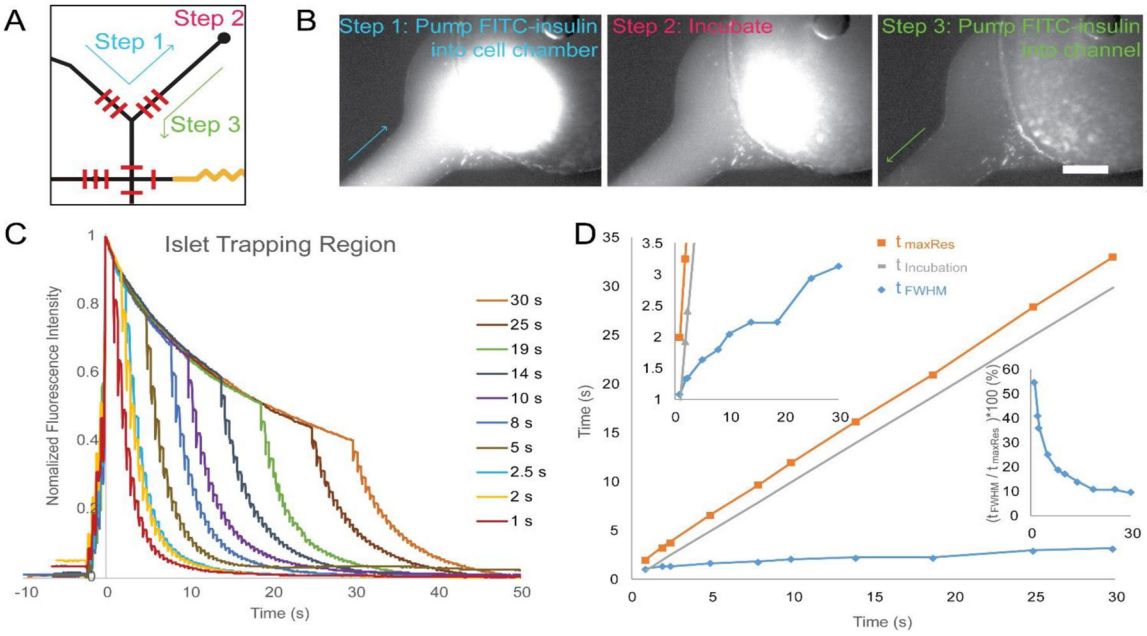

Figure 3.

Insulin diffusion test to determine temporal resolution. **(A)** Procedure of islet mimicking, where FITC-insulin was pumped into the cell chamber, incubated, and pumped back into the channel. **(B)** Example fluorescent images of each step. **(C)** Normalized fluorescence in islet trapping region during the test with various incubation times (1 to 30 s). **(D)** Measured time for fluorescence drop to half of the sampling start point. Top-left inset is zoomed-in plot highlighting the t_{FWHM} (time to reach full-width at half-maximum). Bottom-right inset shows the percentage of the t_{FWHM} in t_{maxRes} (measured best temporal resolution).

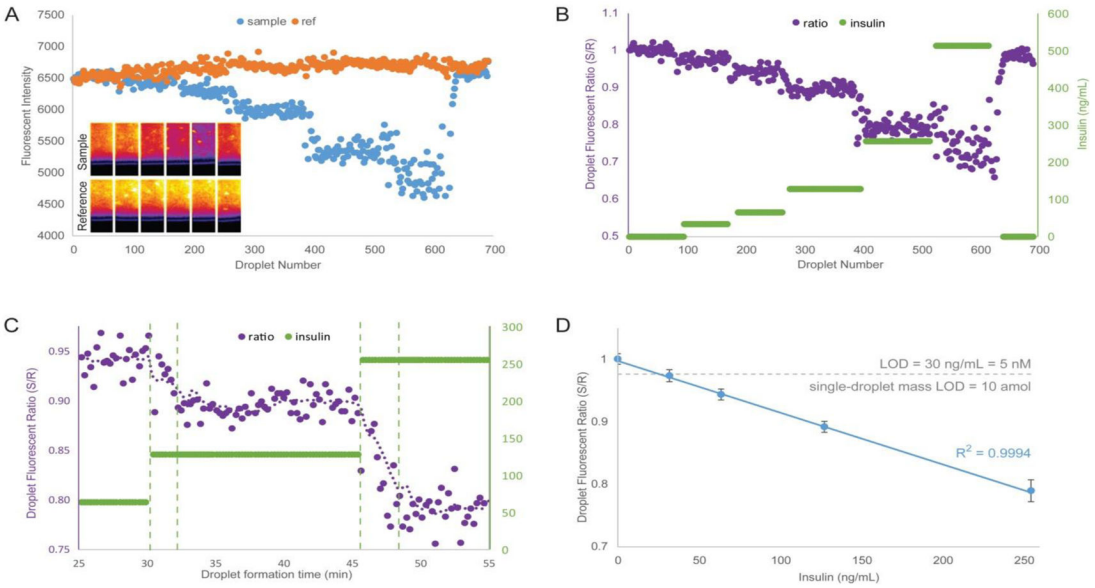

Figure 4.

Homogeneous, mix-and-read insulin quantification within droplets. **(A)** Averaged fluorescence intensities of individual sample (blue) and reference (orange) droplets during calibration, before lock-in analysis. Inset are examples of fluorescent images of the droplets. **(B)** Fluorescence ratios of sample and neighbouring reference droplets (purple). The added insulin concentration is shown in green. A zoomed-in plot **(C)** shows the ratio changing within 2–3 min after exchanging insulin concentration in the bulk reservoir. **(D)** Insulin standard curve; error bars indicate standard deviations of ratios of 20 droplet pairs. Concentration LOD = 30 ng/mL = 5 nM. Single droplet mass LOD = 10 amol.

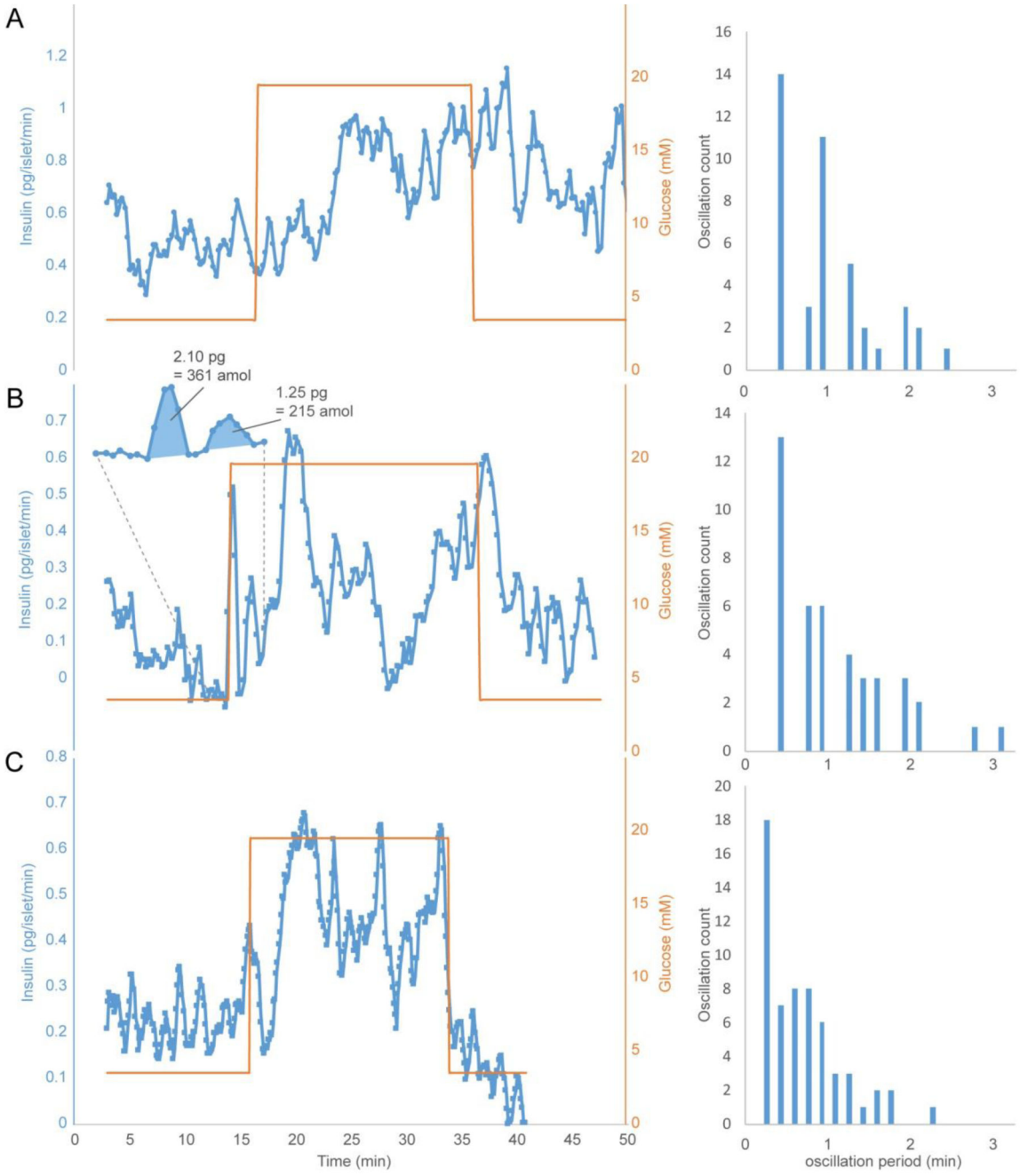

Figure 5.

Insulin secretion from three different single islets **(A, B, C)**, as quantified by our automated, droplet-based sampling and analysis device. The left plots show insulin secretion rates in pg/islet/min (blue) along with the imposed glucose waveforms in mM (orange). The 15-second resolution capabilities of the device allowed observation of both fast and slow insulin oscillations. Zoomed-in data in panel **(B)** shows a 5-minute segment of the data and highlights two bursts of secreted insulin along with the amounts of insulin released in each

burst. The right plots show histograms of the insulin oscillation periods from the corresponding data on the left.